Reactions of Laser-Ablated Rhodium and Iridium Atoms with Nitric Oxide in Neon and Argon. Matrix Infrared Spectra and Density Functional Calculations of $Rh(NO)_{1-3}$, $Ir(NO)_{1-3}$, NRhO, NIrO, $RhNO^+$, and $IrNO^+$

Angelo Citra and Lester Andrews*

Department of Chemistry, University of Virginia, Charlottesville, Virginia 22901

Received: August 21, 2000; In Final Form: October 9, 2000

Laser-ablated rhodium and iridium atoms are reacted with nitric oxide and the products are isolated in solid neon and argon. Neutral nitrosyl complexes $Rh(NO)_{1-3}$ and $Ir(NO)_{1-3}$ are the main products, and weaker bands due to $RhNO^+$, $IrNO^+$, NRhO, and NIrO are also observed. DFT calculations for these products using the BPW91 and B3LYP functionals determine frequencies with the same accuracy found for other metal nitrosyls and are a useful predictive tool. The stretching frequencies observed for the isolated nitrosyls are close to those for analogous nitrosyl species on rhodium and iridium surfaces, which will aid in interpreting vibrational data for surface species.

Introduction

The interaction between rhodium and nitric oxide is important as the metal is incorporated in catalytic converters to decrease emissions of pollutant gases, and numerous experimental and theoretical studies have been made over the past decade.[1−9] The iridium and nitric oxide system has also been investigated.[10−12] Nitric oxide is found to adsorb both molecularly and dissociatively, depending on the temperature, surface coverage, and how the metal catalysts are supported. Many assignments have been made to various rhodium nitrosyl surface species using vibrational data, but these are commonly done without the benefit of the isotopic data required to identify intermediates that lend support to proposed reaction schemes.

In the present work, the reactions between laser-ablated rhodium and iridium atoms and nitric oxide are studied by isolating transient reaction products in solid argon and neon. Experiments are performed using $^{14}N^{16}O$, $^{15}N^{16}O$, $^{15}N^{18}O$, and mixtures of these to determine the stoichiometry of products formed. Density functional theory (DFT) is used to calculate proposed reaction products, both to aid in making assignments and to assess the effectiveness of these calculations. The noble gas matrix system is less complicated than an extended metal surface, and allows unambiguous identification of the important metal nitrosyl products. This information may then be used in understanding the larger rhodium and iridium surface systems. Further, this and the preceding work on matrix-isolated rhodium and iridium carbonyls[13,14] lay the groundwork for a future study of these metal atoms with CO/NO mixtures.

Neutral and charged nitrosyl complexes are formed with each metal which are found to correlate well with vibrational data for the corresponding metal surfaces. No surface counterparts for the isolated $Rh(NO)_3$ and $Ir(NO)_3$ complexes identified in this work have been reported, though future isotopic studies of supported rhodium catalysts may yet reveal such species, as has been found with iron zeolites.[15] In addition, the insertion products NIrO and NRhO are observed, allowing a study of the trends in metal−ligand bond strength by comparison with results for other transition metals.[16−26]

Experimental and Theoretical Methods

The experiment for laser ablation and matrix isolation has been described in detail previously.[27,28] Briefly, the Nd:YAG laser fundamental (1064 nm, 10 Hz repetition rate with 10 ns pulse width) was focused on rotating rhodium and iridium targets (Goodfellow Metals). Laser energies ranging from 5 to 50 mJ/pulse were used. In experiments with neon, a 10% neutral density filter was used to reduce the laser energy. Laser-ablated metal atoms, cations and electrons were co-deposited with nitric oxide at 0.6−0.1% in argon or 0.2−0.02% in neon onto a 7−8 K or 4−5 K CsI window at 2−4 mmol/h for 30 min to 2 h. Several isotopic samples ($^{14}N^{16}O$, Matheson; $^{15}N^{16}O$, MDS isotopes, 99%; $^{15}N^{18}O$, Isotec, 99%) and selected mixtures were used. Infrared spectra were recorded at 0.5 cm^{-1} resolution on a Nicolet 750 spectrometer with 0.1 cm^{-1} accuracy with a HgCdTe detector. Matrix samples were annealed at a range of temperatures (20−45 K in argon, and 6−11 K in neon) and subjected to broadband photolysis by a medium-pressure mercury arc (Philips, 175 W) with the globe removed ($\lambda > 240$ nm).

Density functional theory (DFT) calculations were performed on the rhodium and iridium nitrosyls using the Gaussian 94 program.[29] The BPW91 functional was used in all calculations, while the B3LYP functional was employed for comparison in selected cases.[30−32] The 6-311+G(d) basis set was used to represent nitrogen and oxygen,[33] and the LanL2DZ ECP basis set was used for rhodium and iridium.[34,35]

Results

Absorptions for rhodium and iridium nitrosyl products in pure and mixed isotopic experiments in solid neon and argon are listed in Tables 1−4. Figures 1−8 show spectra in neon and argon matricies in both nitrosyl and nitride-oxide regions. Additional bands due to NO, $(NO)_2$, $(NO)_2^+$, $(NO)_2^-$, NO_2, and NO_2^- common to experiments with laser-ablated metal and nitric oxide are not listed in the tables.[26] The optimized geometries and associated harmonic frequencies of product molecules calculated using DFT are summarized in Tables 5−8, energies

10.1021/jp0029919 CCC: $19.00
Published on Web 12/02/2000

TABLE 1: Infrared Absorptions (cm^{-1}) from Co-deposition of Laser-Ablated Rhodium Atoms with NO in Excess Neon at 4 K

$^{14}N^{16}O$	$^{15}N^{16}O$ [$^{14}N^{16}O/^{15}N^{16}O$]	$^{15}N^{18}O$ [$^{15}N^{16}O/^{15}N^{18}O$]	$^{14}N^{16}O + {}^{15}N^{16}O$	assignment
1957.5	1919.9 [1.0196]	1874.1 [1.0244]	1957.5, 1919.9	$RhNO^+$
1806.4	1769.6 [1.0208]	1731.7 [1.0219]	1806.4, 1769.6	RhNO
1757.7	1724.3 [1.0194]	1682.4 [1.0249]	*b*	$Rh(NO)_3$
1756.2	1721.6 [1.0201]	a	*b*	$Rh(NO)_3$ (site)
1754.8	*a*	1679.6	*b*	$Rh(NO)_3$ (site)
1752.6	1718.7 [1.0197]	1678.3 [1.0241]	*b*	$Rh(NO)_3$ (site)
1746.9	1713.3 [1.0196]	1672.6 [1.0243]	*b*	$Rh(NO)_2$
1742.0	1708.6 [1.0196]	1667.9 [1.0244]	*b*	$Rh(NO)_2$ (site)
967.8	939.4 [1.0302]	939.3 [1.0001]	*a*	NRhO
965.4	936.8 [1.0305]	936.7 [1.0001]	*a*	NRhO (site)

[a] Band was not observed in this experiment. [b] Spectral region too congested to observe bands.

TABLE 2: Infrared Absorptions (cm^{-1}) from Co-deposition of Laser-Ablated Rhodium Atoms with NO in Excess Argon at 7 K

$^{14}N^{16}O$	$^{15}N^{16}O$ [$^{14}N^{16}O/^{15}N^{16}O$]	$^{15}N^{18}O$ [$^{15}N^{16}O/^{15}N^{18}O$]	$^{14}N^{16}O + {}^{15}N^{16}O$	assignment
1801.8	1766.3 [1.0201]	1725.7 [1.0235]	*b*	$Rh(NO)_2$
1796.3	1761.1 [1.0200]	1720.4 [1.0237]	*b*	$Rh(NO)_2$ (site)
1775.1[d]	1738.8[d] [1.0209]	*b*	*b*	RhNO
1749.0	1715.4 [1.0196]	*a*	*b*	$Rh(NO)_3$
1745.9	1712.8 [1.0193]	1671.3 [1.0248]	1745.9, 1731.4, 1721.2, 1712.8	$Rh(NO)_3$ (site)
b	1711.6	*b*	*b*, 1730.1, 1720.0, 1711.6	$Rh(NO)_3$ (site)
1743.4	1709.6 [1.0198]	1669.5 [1.0240]	*b*, 1709.6	$Rh(NO)_3$ (site)
1740.9	1707.9 [1.0193]	1666.4 [1.0249]	1740.9, 1726.6, 1715.6, 1708.0	$Rh(NO)_3$ (site)
1736.5	1702.8 [1.0198]	1662.8 [1.0241]	1736.5, *b*, 1702.9	$Rh(NO)_2$
1734.3	1701.2 [1.0195]	1660.0 [1.0248]	1734.3, *b*, 1701.2	$Rh(NO)_2$ (site)
1708.9	1673.0 [1.0215]	*a*	*a*	$Rh_x(NO)_y$
1634.9	1603.8 [1.0194]	*a*	1634.9, 1603.8	
1554.5	1524.5 [1.0197]	*a*	*a*	
1553.4	1523.3 [1.0198]	*a*	*a*	
1543.1	1514.3 [1.0190]	1477.3 [1.0250]	*b*	
1527.4	1495.5 [1.0213]	*a*	*b*	
1524.6	1492.3 [1.0216]	*a*	*b*	
1521.8	1490.2 [1.0212]	*a*	1521.9, 1490.2	
964.2	935.7 [1.0305]	935.6 [1.0001]	964.2, 935.7	NRhO
813.7	813.6 [1.0001]	773.6 [1.0517]	813.7	NRhO

[a] Band not observed in this experiment. [b] Spectral region too congested to observe bands. [c] Unresolved bands. [d] Bands obscured, values taken from ref 36.

TABLE 3: Infrared Absorptions (cm^{-1}) from Co-deposition of Laser-Ablated Iridium Atoms with NO in Excess Neon at 4 K

$^{14}N^{16}O$	$^{15}N^{16}O$ [$^{14}N^{16}O/^{15}N^{16}O$]	$^{15}N^{18}O$ [$^{15}N^{16}O/^{15}N^{18}O$]	$^{14}N^{16}O + {}^{15}N^{16}O$	assignment
1993.3	1952.8 [1.0207]	*a*	1993.3, 1952.8	$IrNO^+$ (site)
1990.0	1949.5 [1.0208]	*a*	1990.0, 1949.5	$IrNO^+$
1851.1	1810.6 [1.0224]	*b*	*b*, 1851.1	IrNO
1850.0	1809.4 [1.0224]	*b*	*b*, 1850.0	IrNO (site)
1757.5	1722.6 [1.0203]	*c*	*b*	$Ir(NO)_3$ (site)
1756.1	1721.4 [1.0202]	*c*	*b*	$Ir(NO)_3$ (site)
1755.3	1720.6 [1.0202]	*c*	*b*	$Ir(NO)_3$ (site)
1753.7	1718.9 [1.0202]	1669.5 [1.0296]	*b*	$Ir(NO)_3$
1744.6	*a*	1671.7	*b*	?
1699.7	1668.9 [1.0185]	1630.6 [1.0235]	*a*	$Ir_x(NO)_y$
1696.9	1664.7 [1.0193]	a	*a*	$Ir_x(NO)_y$
1686.9	1657.7 [1.0176]	a	*a*	$Ir_x(NO)_y$
1684.6	1654.4 [1.0183]	1612.9 [1.0257]	*a*	$Ir_x(NO)_y$
1681.1	1652.0 [1.0176]	1607.2 [1.0279]	*a*	$Ir_x(NO)_y$
1001.8	973.5 [1.0291]	a	*a*	?
994.6	968.8 [1.0266]	a	*a*	NIrO
868.9	866.4 [1.0029]	830.0 [1.0439]	868.9, 866.4	NIrO

[a] Band not observed in this experiment. [b] Spectral region too congested to observe bands. [c] Unresolved bands.

of reactions are in Table 9, and additional force constant information is included in Tables 10 and 11.

Discussion

New product molecules are identified by isotopic substitution and DFT calculations as follows.

RhNO. A weak, sharp band is observed at 1806.4 cm^{-1} in neon that grows significantly during annealing and photolysis and exhibits a doublet of peaks in mixed isotopic experiments, indicating that only one nitrosyl group is present (Figure 1). The $^{14}N^{16}O/^{15}N^{16}O$ ratio of 1.0208 is typical for metal nitrosyls,[16−26] higher than the value of 1.0179 for isolated nitric oxide due to coupling with the M−N vibration. Conversely, the $^{15}N^{16}O/^{15}N^{18}O$ ratio of 1.0219, which indicates the degree of oxygen participation in the mode, is lower than the value of 1.0276 for the isolated molecule. The RhNO molecule was previously observed in argon at 1775.1 cm^{-1} (^{14}N) and 1738.8 cm^{-1} (^{15}N) in the matrix isolation study of rhodium and nitrogen,

TABLE 4: Infrared Absorptions (cm^{-1}) from Co-deposition of Laser-Ablated Iridium Atoms with NO in Excess Argon at 7 K

$^{14}N^{16}O$	$^{15}N^{16}O$ [$^{14}N^{16}O/^{15}N^{16}O$]	$^{15}N^{18}O$ [$^{15}N^{16}O/^{15}N^{18}O$]	$^{14}N^{16}O + {}^{15}N^{16}O$	assignment
3550.3	3480.3 [1.0201]	*a*	*a*	$Ir(NO)_3$
3479.9	3411.1 [1.0202]	*a*	3479.9, 3459.8, 3423.5, 3411.1	$Ir(NO)_3$
3475.5	3407.4 [1.0200]	*a*	3475.5, 3455.3, 3419.8, 3407.4	$Ir(NO)_3$ (site)
1838.7	1798.6 [1.0222]	1763.6 [1.0198]	*b*, 1798.8	IrNO (site)
1837.4	1797.2 [1.0224]	*a*	*b*, 1797.2	IrNO (site)
1835.8	1795.6 [1.0224]	1760.9 [1.0198]	1835.8, 1795.6	IrNO (site)
1833.7	1793.8 [1.0222]	1759.0 [1.0198]	1833.7, 1793.7	IrNO
1745.5	1711.0 [1.0202]	1671.7 [1.0235]	*b*, 1729.6, 1719.5, 1711.0	$Ir(NO)_3$
1743.2	1708.4 [1.0204]	1669.5 [1.0233]	1743.2, 1721.3, 1708.4	$Ir(NO)_2$
1741.4	1707.0 [1.0202]	1667.9 [1.0234]	1741.4, *b*, 1667.9	$Ir(NO)_2$ (site)
1737.3	1702.6 [1.0204]	1663.7 [1.0234]	1737.3, 1715.8, 1663.7	$Ir(NO)_2$ (site)
1710.8	1676.9 [1.0202]	1638.7 [1.0233]	*a*	$Ir_x(NO)_y$
1709.0	1675.4 [1.0205]	1637.2 [1.0233]	*a*	$Ir_x(NO)_y$
1692.1	1660.6 [1.0190]	1619.4 [1.0254]	*a*	$Ir_x(NO)_y$
1086.0	1085.7 [1.0003]	1059.4 [1.0248]	1085.8	?
977.3	951.9 [1.0267]	946.9 [1.0053]	977.3, 951.9	NIrO
975.3	950.3 [1.0263]	944.7 [1.0059]	975.3, 950.3	NIrO (site)
852.6	849.8 [1.0033]	813.7 [1.0444]	852.6, 849.8	NIrO (site)
850.6	848.0 [1.0031]	811.6 [1.0448]	850.6, 848.0	NIrO

[a] Band not observed in this experiment. [b] Spectral region too congested to observe bands. [c] Unresolved bands.

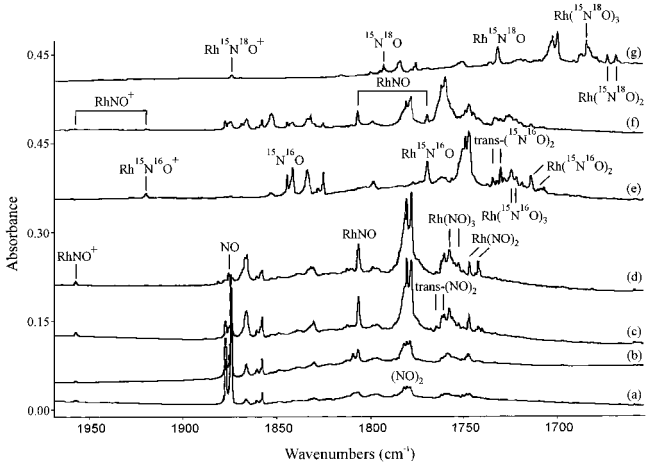

Figure 1. Infrared spectra in the 1960−1660 cm^{-1} region for laser-ablated rhodium atoms after (a) 50 min deposition with 0.12% NO in neon, (b) annealing to 8 K, (c) annealing to 11 K, (d) annealing to 12 K, and after (e) 25 min deposition with 0.13% $^{15}N^{16}O$ in neon and annealing to 10 K, (f) 25 min deposition with 0.12% NO + 0.12% $^{15}N^{16}O$ in neon and annealing to 10 K, and (g) 25 min deposition with 0.11% $^{15}N^{18}O$ in neon and annealing to 10 K.

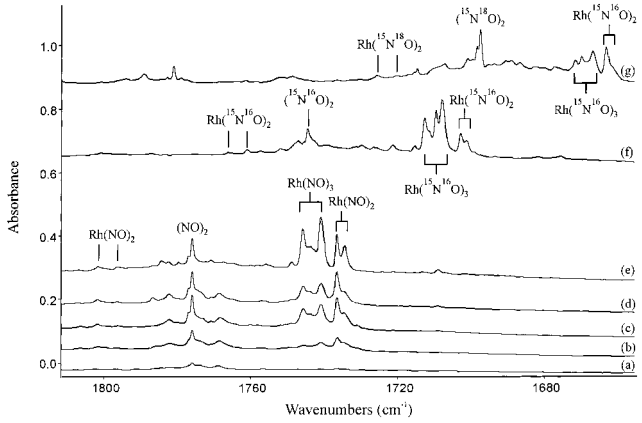

Figure 2. Infrared spectra in the 1810−1660 cm^{-1} region for laser-ablated rhodium atoms after (a) 30 min deposition with 0.3% NO in argon, (b) annealing to 25 K, (c) annealing to 30 K, (d) 26 min photolysis, (e) annealing to 45 K, and after (f) 30 min deposition with 0.25% $^{15}N^{16}O$ in argon and annealing to 45 K, and (g) 50 min deposition with 0.25% $^{15}N^{18}O$ in argon and annealing to 45 K.

where nitric oxide was present as a trace impurity.[36] However, the greater concentration of nitric oxide used in the present argon matrix work gives $(NO)_2$, which covers this region.

Both density functionals predict singlet ground states with slightly bent geometries, ∠RhNO = 157.1° (BPW91) and 145.5° (B3LYP); the linear geometries have imaginary bending frequencies. Comparison with previous results for other metal nitrosyl systems suggests that the nitrosyl stretching frequency for RhNO is underestimated with both functionals: the BPW91 value of 1785.6 cm^{-1} is close to the experimental value but is 20 cm^{-1} too low, whereas similar calculations for other metal nitrosyls tend to give values 30−40 cm^{-1} too high.[24,25] Similarly, the B3LYP value of 1807.3 cm^{-1} is in excellent agreement with experiment, but in other cases the calculated frequency is too high and must be scaled down by 0.94−0.96.[24,25] The calculated $^{14}N^{16}O/^{15}N^{16}O$ and $^{15}N^{16}O/^{15}N^{18}O$ isotopic ratios of 1.0208 and 1.0234 (BPW91) and 1.0200 and 1.0249 (B3LYP) are in reasonable agreement with experiment; the BPW91 values are slightly closer to the measured values. Other electronic states were calculated by altering orbital occupations and repeating the geometry optimizations, but these were higher in energy with frequencies in greater error. The calculation was repeated with MP2, and in this case the optimized geometry is linear with a nitrosyl stretching frequency of 1858.1 cm^{-1}. This is in greater error than the DFT results, but the isotopic ratios of 1.0213 and 1.0226 calculated with MP2 are in slightly better agreement with experiment. These differences can be attributed to the linear geometry, which maximizes the $^{14}N^{16}O/^{15}N^{16}O$ ratio and minimizes the $^{15}N^{16}O/^{15}N^{18}O$ ratio due to the greater mechanical coupling between the M−N and N−O stretching modes. These results suggest that the linear geometry is correct, and that the DFT calculations erroneously predict a slightly bent geometry, resulting in lower calculated frequencies.

Rh(NO)$_3$. Sharp bands are observed at 1745.9, 1743.4, and 1740.9 cm^{-1} in argon that increases significantly on annealing and each exhibit a quartet of bands in the mixed $^{14}N^{16}O$ + $^{15}N^{16}O$ experiment (Figures 2 and 3), with intermediate components weaker than the pure isotope bands. This is diagnostic of a molecule with a 3-fold rotation axis, like Co(NO)$_3$,[26] and the bands are therefore assigned to Rh(NO)$_3$ in different matrix sites. Unlike Ir(NO)$_3$ described below, no overtone or combination bands are observed, and no estimate for the symmetric stretching mode can be made. The corresponding neon bands are at 1757.7 and 1752.6 cm^{-1}, and the $^{14}NO/^{15}NO$ and $^{15}NO/$

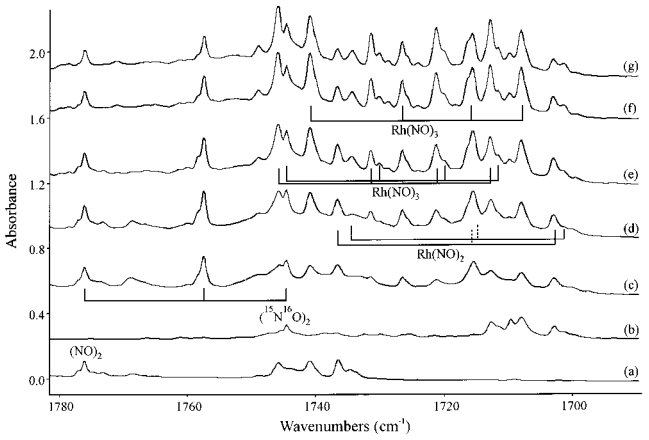

Figure 3. Infrared spectra in the 1780−1690 cm^{-1} region for laser-ablated rhodium atoms after (a) 30 min deposition with 0.2% NO in argon and annealing to 35 K, (b) 30 min deposition with 0.25% ^{15}N^{16}O in argon and annealing to 40 K, (c) 60 min deposition with 0.15% NO + 0.15% ^{15}N^{16}O in argon and annealing to 25 K, and after (d) annealing to 30 K, (e) annealing to 35 K, (f) annealing to 40 K, and (g) after annealing to 43 K.

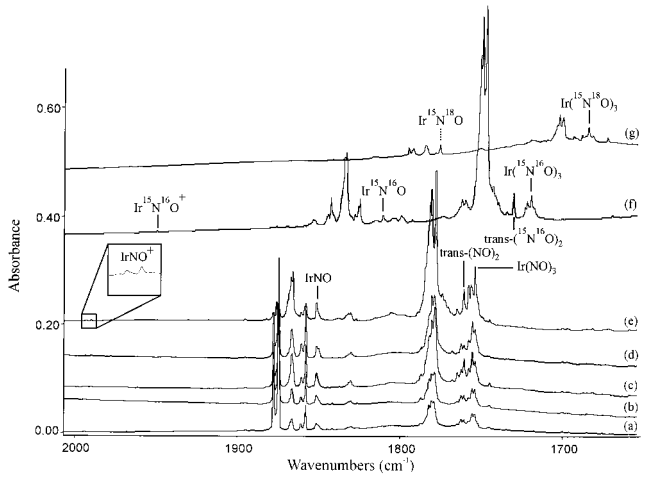

Figure 4. Infrared spectra in the 2000−1660 cm^{-1} region for laser-ablated iridium atoms after (a) 50 min deposition with 0.12% NO in neon, (b) annealing to 7 K, (c) annealing to 10 K, (d) 18 min photolysis, (e) annealing to 12 K, and after (f) 50 min deposition with 0.17% ^{15}N^{16}O in neon and annealing to 11 K, and (g) 50 min deposition with 0.11% ^{15}N^{18}O in neon and annealing to 12 K.

^{15}N^{18}O isotopic ratios of 1.0194 and 1.0249 are almost identical to those in argon (Figure 1). However, the neon spectra in this region are too congested by absorptions due to $(NO)_2$, $Rh(NO)_2$, and $Rh(NO)_3$ in the mixed isotope experiment for the intermediate components of $Rh(NO)_3$ to be distinguished.

The singlet and triplet states of $Rh(NO)_3$ are calculated to be almost identical in energy. However, the geometry is approximately trigonal planar (D_{3h}) for the singlet state, with linear RhNO subunits, whereas the triplet state geometry is essentially planar but with bent RhNO subunits (C_{3h}). This causes the degenerate stretching frequency for the singlet state (1779.7 cm^{-1}) to be higher than that for the triplet state (1744.8 cm^{-1}). The former is 30.7 cm^{-1} higher than the 1749.0 cm^{-1} band observed in argon, and is more in line with previous results for metal nitrosyls.[24,25] Note that the calculated geometries are not exactly D_{3h} or C_{3h}. Such symmetry breaking is commonly found for molecules of high symmetry,[37] and small differences in bond lengths and artificially nondegenerate frequencies are averaged in Tables 5−8.

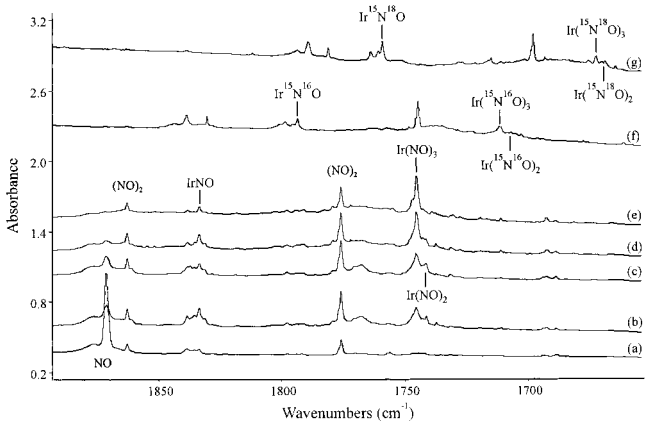

Figure 5. Infrared spectra in the 1900−1650 cm^{-1} region for laser-ablated iridium atoms after (a) 60 min deposition with 0.3% NO in argon, (b) annealing to 25 K, (c) after 25 min photolysis, (d) annealing to 30 K, (e) annealing to 43 K, and after (f) 30 min deposition with 0.25% ^{15}N^{16}O in argon and annealing to 40 K, and (g) 30 min deposition with 0.2% ^{15}N^{18}O in argon and annealing to 40 K.

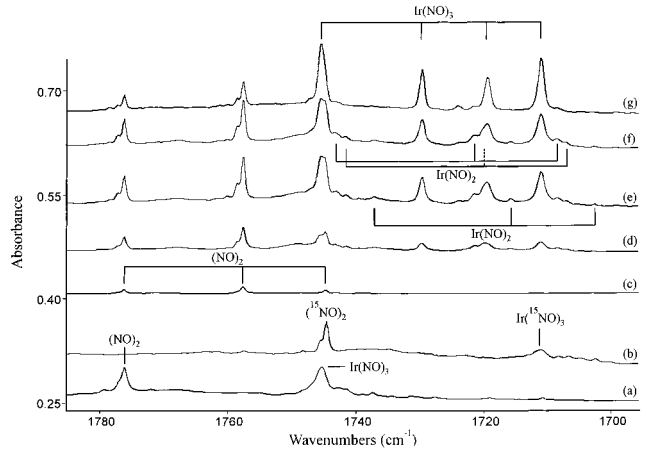

Figure 6. Infrared spectra in the 1785−1695 cm^{-1} region for laser-ablated iridium atoms after (a) 30 min deposition with 0.3% NO in argon and annealing to 40 K, (b) 30 min deposition with 0.25% ^{15}N^{16}O in argon and annealing to 40 K, and after (c) 60 min deposition with 0.1% NO + 0.1% ^{15}N^{16}O in argon, (d) annealing to 25 K, (e) annealing to 30 K, (f) 20 min photolysis, and (g) annealing to 40 K.

$Rh(NO)_2$. Two bands at 1736.7 and 1734.3 cm^{-1} in argon grow in during low-temperature annealing but decrease on the highest annealing temperatures (Figure 2). These bands have isotopic ratios similar to those for the bands assigned to $Rh(NO)_3$, but the mixed isotopic data indicates that these lower frequency bands are due to $Rh(NO)_2$, and not two additional matrix sites of $Rh(NO)_3$ (Figure 3). The bands due to Rh(^{14}N^{16}O)(^{15}N^{16}O)$_2$ and Rh(^{14}N^{16}O)$_2$(^{15}N^{16}O) for the three matrix sites of $Rh(NO)_3$ are observed as shown. If the bands at 1736.7 and 1734.3 cm^{-1} were also due to the trinitrosyl complex, then the corresponding Rh(^{14}N^{16}O)(^{15}N^{16}O)$_2$ band should be observed in the region between the mixed isotope bands at 1726.6 and 1721.2 cm^{-1}, but no such band is present. However, if these and the ^{15}N^{16}O counterparts at 1702.9 and 1701.3 cm^{-1} are due to $Rh(NO)_2$, then the intermediate band due to Rh(^{14}N^{16}O)-(^{15}N^{16}O) is expected to fall at ~1715 cm^{-1}, a few wavenumbers below the midpoint of the pure isotope bands, as is typically the case for this type of molecule. This would be completely obscured by the peak at 1715.6 cm^{-1} due to Rh(^{14}N^{16}O)$_2$-(^{15}N^{16}O), but can be detected indirectly by the increase in the intensity of the 1715.6 cm^{-1} band relative to the other bands in the quartet. It is also apparent from the change in intensity of

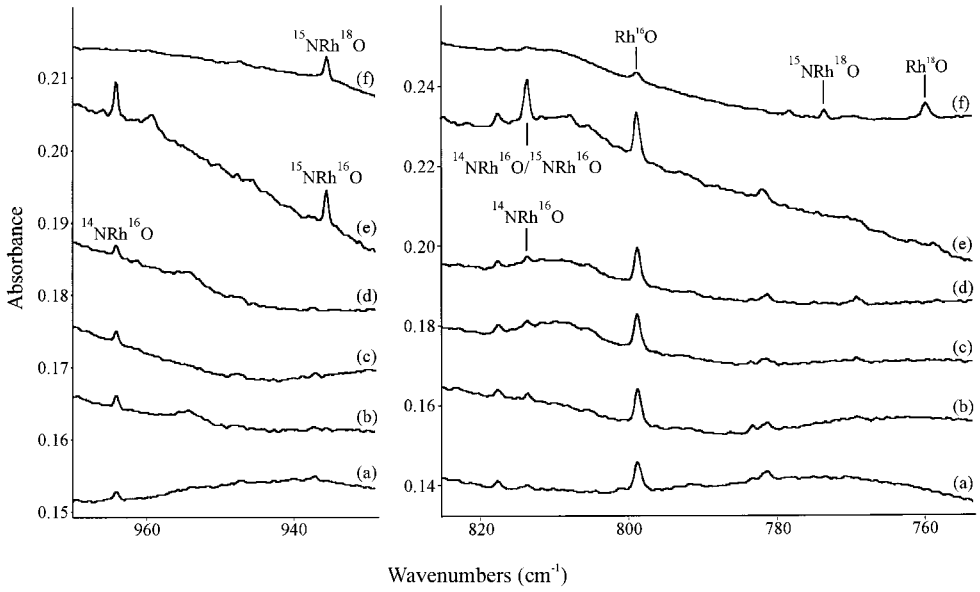

Figure 7. Infrared spectra in the 970−930 and 825−755 cm^{-1} regions for laser-ablated rhodium atoms after (a) 60 min deposition with 0.6% NO in argon, (b) annealing to 25 K, (c) 25 min photolysis, (d) annealing to 30 K, and after (e) 60 min deposition with 0.15% NO + 0.15% $^{15}N^{16}O$ in argon and annealing to 30 K, and (f) 50 min deposition with 0.25% $^{15}N^{18}O$ in argon and annealing to 30 K.

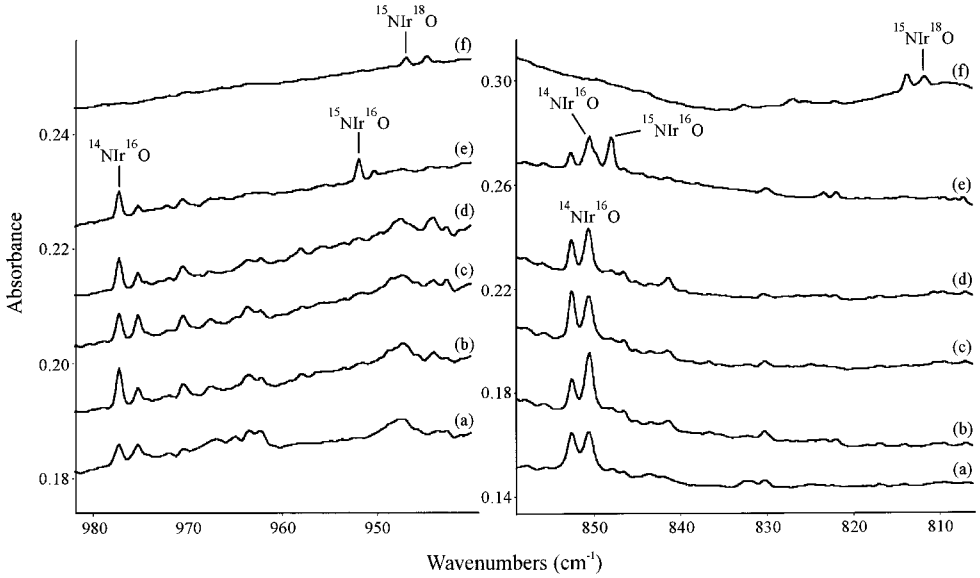

Figure 8. Infrared spectra in the 980−940 and 860−810 cm^{-1} regions for laser-ablated iridium atoms after (a) 60 min deposition with 0.3% NO in argon, (b) annealing to 25 K, (c) 25 min photolysis, (d) annealing to 30 K, and after (e) 60 min deposition with 0.1% NO + 0.1% $^{15}N^{16}O$ in argon and annealing to 30 K, and (f) 55 min deposition with 0.25% $^{15}N^{18}O$ in argon and annealing to 30 K.

this band during annealing, which is slightly different to the other bands in the quartet. This is clear in the later annealing cycles where the bands at 1736.7, 1734.3, 1715.6, 1702.8, and 1701.2 cm^{-1} decrease, whereas the bands at 1740.9, 1726.6, and 1708.0 cm^{-1} increase. These observations support the assignment of the observed bands to $Rh(NO)_2$. The most likely candidate bands for this molecule in neon are at 1746.9 and 1742.0 cm^{-1}, red-shifted from the broad band at 1752.6 cm^{-1} assigned to $Rh(NO)_3$, though the mixed isotopic data in neon are too congested for any information regarding $Rh(NO)_2$ or $Rh(NO)_3$ to be obtained.

The lowest energy state calculated for $Rh(NO)_2$ using the BPW91 functional is $^2B_1$, a planar structure with nonlinear nitrosyl linkages. Nonplanar structures were calculated, but are considerably higher in energy. Both linear and bent quartet states were calculated to be much higher in energy, and $^2B_1$ is identified as the ground state. The asymmetric stretching frequency of 1764.0 cm^{-1} is 27.5 cm^{-1} higher than the argon value, supporting the assignment. The $^{14}N^{16}O/^{15}N^{16}O$ and $^{15}N^{16}O/^{15}N^{18}O$ ratios of 1.0201 and 1.0248 are in good agreement with the experimental values of 1.0198 and 1.0241, and the antisymmetric stretching frequency in the mixed isotope Rh-($^{14}N^{16}O$)($^{15}N^{16}O$) is calculated to be 1741.7 cm^{-1}, 5 cm^{-1} below the midpoint of the pure isotope bands, as expected from the mixed $^{14}N^{16}O$ + $^{15}N^{16}O$/Ar experiment. The results of the B3LYP calculations are more complicated, however. The $^2B_1$ state is calculated to be much lower in energy than the linear quartet state, and has an antisymmetric stretching frequency of 1797.8 cm^{-1}, requiring a scale factor of 0.966 to fit the argon value. However, this state also has a large imaginary frequency which corresponds to an out-of-plane deformation mode. When the calculation is repeated for a nonplanar structure, the rhodium atom moves out of the plane of the molecule during the geometry optimization to give a structure of C_s symmetry. Both $^2A'$ and $^2A''$ states were calculated, but the latter state is much higher in energy. The $^2A'$ state is marginally lower in energy

TABLE 5: Geometries, Energies, and Frequencies Calculated for Neutral and Ionic Rhodium Nitrosyls Using DFT (BPW91/LanL2DZ/6-311+G(d))

molecule	state (point group)	relative energies (kJ/mol)[a]	$\langle S^2 \rangle$	geometry (Å deg)	frequencies (cm^{-1}) [intensities (km/mol)]
RhNO	$^1A'$ (C_s)	0		RhN: 1.735; NO: 1.175 ∠RhNO: 157.1	1785.6 [558], 609.2 [0], 140.4 [11]
	$^3A'$ (C_s)	+90	2.0000	RhN: 1.868; NO: 1.186 ∠RhNO: 128.3	1661.5 [796], 562.2 [6], 262.9 [5]
NRhO	$^1A'$ (C_s)	+203		RhN: 1.661; RhO: 1.768 ∠NRhO: 139.4	1017.2 [103], 826.1 [92], 195.2 [20]
	$^1A''$ (C_s)	+271	0.1485	RhN: 1.675; RhO: 1.805 ∠NRhO: 123.5	956.0 [29], 680.7 [41], 226.2 [9]
	$^3A'$ (C_s)	+288	2.0000	RhN: 1.717; RhO: 1.812 ∠NRhO: 113.6	883.2 [4], 679.0 [38], 265.5 [2]
	$^3A''$ (C_s)	+255	2.0000	RhN: 1.678; RhO: 1.794 ∠NRhO: 124.4	955.4 [32], 717.5 [45], 233.0 [9]
$RhNO^+$	$^2\Sigma^+$ ($C_{\infty v}$)	0	0.7500	RhN: 1.774; NO: 1.135 ∠RhNO: 180.0	1990.8 [452], 538.4 [13], 200.9 [6]x2
	$^4A'$ (C_s)	+134	3.7500	RhN: 1.986; NO: 1.150 ∠RhNO: 144.8	1862.8 [583], 394.3 [14], 262.2 [2]
$Rh(NO)_2$	$^2B_1$ (C_{2v})	0	0.7500	RhN: 1.815; NO: 1.174 ∠RhNO: 163.2 ∠NRhN: 128.0 ϕ(ONRhN): 0.0	1823.5 [194], 1764.0 [1565], 570.9 [4], 488.4 [2], 485.5 [2]...48.6 [5]
	$^2A''$ (C_s)	+83	0.7506	RhN: 1.868; NO: 1.186 ∠RhNO: 135.0 ∠NRhN: 116.6 ϕ(ONRhN): 81.3	1696.1 [286], 1640.9 [1410], 549.9 [3]...−80.3 [0], −521.1 [141]
	$^4\Sigma^-_g$ ($C_{\infty v}$)	+85	3.7502	RhN: 1.848; NO: 1.180 ∠RhNO: 180.0 ∠NRhN: 180.0	1813.1 [0], 1735.8 [1724], 492.4 [9]x2, 460.4 [0], 418.3 [26]...43.0 [1]
	$^4A_2$	+209	3.7500	RhN: 1.873; NO: 1.184 ∠RhNO: 165.8 ∠NRhN: 119.7 ϕ(ONRhN): 0.0	
$Rh(NO)_3$	$''^1A''$ (D_{3h})	0		RhN: 1.851; NO: 1.169 ∠RuNO: 180.0 ∠NRuN: 120.0	1848.4 [0], 1779.9 [1564]x2, 543.7 [27], 543.0 [39]x2, 459.5 [0], 430.2 [29]x2...−20.1 [0]
	$''^3A''$ (C_{3h})	+1	2.0013	RhN: 1.879; NO: 1.174 ∠RhNO: 155.1 ∠NRhN: 120.0	1808.5 [0], 1744.8 [1486]x2, 461.1 [3]x2, 451.9 [0]...−10.9 [0]

TABLE 6: Geometries, Energies, and Frequencies Calculated for Selected Neutral and Ionic Rhodium Nitrosyls Using DFT (B3LYP/LanL2DZ/6-311+G(d))

molecule (ground state) [relative energy, kJ/mol]	$\langle S^2 \rangle$	geometry (Å deg)	frequencies (cm^{-1}) [intensities (km/mol)]	scale factors: argon	scale factors: neon
RhNO ($^1A'$) [0]		RhN: 1.741; NO: 1.167 ∠RhNO: 145.5	1807.4 [713], 648.2 [1], 174.2 [1]		0.999
NRhO ($^1A'$) [+249]		RhN: 1.639; RhO: 1.756 ∠NRhO: 143.1	1060.5 [143], 865.3 [143], 207.4 [31]	0.909 0.940	0.913
NRhO ($^1A''$) [+286]	0.4134	RhN: 1.649; RhO: 1.850 ∠NRhO: 122.8	994.5 [30], 557.3 [20], 204.1 [14]		
NRhO ($^3A'$) [+342]	2.0368	RhN: 1.721; RhO: 1.781 ∠NRhO: 125.8	718.6 [31], 682.8 [13], 201.2 [16]		
NRhO ($^3A''$) [+387]	2.0089	RhN: 1.745; RhO: 1.818 ∠NRhO: 123.2	822.4 [80], 538.9 [87], 134.1 [23]		
$RhNO^+$ ($^2\Sigma^+$)	0.7501	RhN: 1.789; NO: 1.118 ∠RhNO: 180.0	2087.4 [643], 20.9 [21], 191.0 [5]		0.938
$Rh(NO)_2$ ($^2B_1$) [+2]	0.7541	RhN: 1.822; NO: 1.159 ∠NRhN: 132.7 ∠RhNO: 166.8 ϕ(ONRhN): 0.0	1903.5 [200], 1835.1 [2078], 549.5 [4], 484.7 [1]... ∠199.9 [15]	0.946	0.953
$Rh(NO)_2$ ($^2A'$) [0]	0.7533	RhN: 1.834; NO: 1.163 ∠NRhN: 126.1 ∠RhNO: 149.8 ϕ(ONRhN): 34.2	1868.8 [264], 1797.8 [1705], 515.4 [0], 425.6 [1]...45.9 [1]		
$Rh(NO)_2$ ($^4\Sigma^-_g$) [+52]	3.7543	RhN: 1.854; NO: 1.169 ∠NRhN: 180.0 ∠RhNO: 180.0	1873.4 [0], 1795.2 [2195], 523.0 [12]x2, 453.2 [0], 419.9 [77]...55.5 [1]x2		
$Rh(NO)_3$ ($''^1A''$)		RhN: 1.851; NO: 1.154 ∠NRhN: 120.0 ∠RhNO: 180.0	1931.3 [0], 1846.5 [2099]x2, 567.3 [33], 550.4 [38]x2, 463.1 [0], ∠41.1 [0]	0.947	0.952

TABLE 7: Geometries, Energies, and Frequencies Calculated for Neutral and Ionic Iridium Nitrosyls Using DFT (BPW91/LanL2DZ/6-311+G(d))

molecule	state (point group)	relative energies (kJ/mol)[a]	$\langle S^2 \rangle$	geometry (Å deg)	frequencies (cm^{-1}) [intensities (km/mol)]
IrNO	$^1\Sigma^+$ ($C_{\infty v}$)	0		IrN: 1.677; NO: 1.174 ∠IrNO: 180.0	1878.9 [499], 689.7 [4], 359.4 [13]x2
	$^1\Delta$ ($C_{\infty v}$)	+123	0.0429	IrN: 1.784; NO: 1.164 ∠IrNO: 180.0	
	$^3A'$	+53	2.0000	IrN: 1.793; NO: 1.182 ∠IrNO: 142.3	1706.9 [755], 654.6 [8], 343.0 [12]
NIrO	$^1A'$ (C_s)	+69	/	IrN: 1.671; IrO: 1.754 ∠NIrO: 120.3	1076.0 [17], 856.8 [77], 299.6 [0]
	$^1A''$ (C_s)	+86	0.0635	IrN: 1.682; IrO: 1.765 ∠NIrO: 124.5	1046.3 [11], 816.1 [49], 276.9 [1]
	$^3A'$ (C_s)	+120	2.0000	IrN: 1.683; IrO: 1.781 ∠NIrO: 140.1	1035.6 [30], 800.2 [69], 258.9 [3]
	$^3A''$ (C_s)	+64	2.0000	IrN: 1.681; IrO: 1.764 ∠NIrO: 125.3	1050.2 [12], 822.1 [49], 275.4 [1]
$IrNO^+$	$^2\Delta$ ($C_{\infty v}$)	0	0.7501	IrN: 1.733; NO: 1.138 ∠IrNO: 180.0	2023.9 [434], 624.6 [8], 338.2 [8]x2
	$^2\Sigma^+$ ($C_{\infty v}$)	+28	0.7500	IrN: 1.721; NO: 1.143 ∠IrNO: 180.0	1993.1 [418], 637.6 [8], 369.2 [6]x2
	$^4A''$ (C_s)	+113	3.7500	IrN: 1.875; NO: 1.149 ∠IrNO: 142.8	1843.6 [112], 554.9 [17], 346.7 [13]
$Ir(NO)_2$	$^2B_1$ (C_{2v})	0	0.7500	IrN: 1.788; NO: 1.177 ∠IrNO: 166.1 ∠NIrN: 138.0 ϕ(ONIrN): 0.0	1846.6 [130], 1779.0 [1480], 634.6 [2], 538.6 [3], 520.9 [0]... 84.7 [1]
	$^2A_1$ (C_{2v})	+15	0.7500	IrN: 1.794; NO: 1.176 ∠IrNO: 164.1 ∠NIrN: 142.9 ϕ(ONIrN): 0.0	1848.0 [119], 1778.2 [1419], 588.9 [3], 521.9 [1], 474.6 [0], 409.7 [9]...74.9 [1]
	$(\pi)^2(\delta)^1$ ($D_{\infty h}$)	+74	3.7500	IrN: 1.827; NO: 1.179 ∠IrNO: 180.0 ∠NIrN: 180.0	1848.6 [0], 1722.8 [1564], 541.9 [0], 439.5 [11]...66.3 [0]
$Ir(NO)_3$	$''^1A''$ (D_{3h})	0		IrN: 1.823; NO: 1.174 ∠IrNO: 180.0 ∠NIrN: 120.0	1841.4 [0], 1781.0 [1377]x2, 591.1 [63]x2, 539.5 [39], 538.9 [0],457.2 [42]x2...51.6 [0]
	$''^3A''$ (D_{3h})	+11	2.0007	IrN: 1.835; NO: 1.178 ∠IrNO: 180.0 ∠NIrN: 120.0	1819.5 [0], 1768.4 [1254]x2, 533.7 [6]x2, 521.2 [0], 472.3 [4]...42.4 [0]

than the planar $^2B_1$ state and has only real frequencies. However, the nitrosyl stretching frequencies are considerably lower and do no fit the experimental data as well. It is most likely that the $^2B_1$ state is correct, as found with the BPW91 functional, but that the B3LYP calculation is deficient and erroneously predicts a nonplanar geometry. This is similar to the calculations for RhNO, which was optimized to a bent structure with both functional when a linear geometry is more likely to be correct.

Weak, broad bands observed at 1801.8 and 1796.3 cm^{-1} in argon are appropriate for assignment to the symmetric stretching mode of $Rh(NO)_2$ in different matrix sites. Corresponding $^{15}N^{16}O$ and $^{15}N^{18}O$ bands give $^{14}N^{16}O/^{15}N^{16}O$ and $^{15}N^{16}O/^{15}N^{18}O$ ratios of 1.0201 and 1.0235, respectively. The isotopic ratios for the more intense antisymmetric mode were 1.0198 and 1.0241, indicating that the symmetric stretching mode has a slightly greater nitrogen motion and lesser oxygen motion than the asymmetric mode. The DFT results are consistent with this; the symmetric stretching frequency is calculated to be 1823.5 cm^{-1} and the $^{14}N^{16}O/^{15}N^{16}O$ and $^{15}N^{16}O/^{15}N^{18}O$ ratios for the symmetric stretching mode are 1.0203 and 1.0244, respectively (BPW91), compared to the ratios 1.0201 and 1.0248 for the antisymmetric mode. The same trend is found with the B3LYP functional: the ratios for the symmetric nitrosyl stretching mode, 1.0195 and 1.0257, are higher and lower than the 1.0191 and 1.0264 ratios for the asymmetric mode, respectively. Note that these ratios were calculated for the $^2A'$ state, and are probably in greater error than those calculated using BPW91 because the nonplanar geometry calculated using B3LYP is incorrect, which alters the mechanics of the mode. In addition, the relative intensities of 1:8 (BPW91) and 1:7 (B3LYP) are in good agreement with the observed ratio of 1:9. This lends more support to the assignment of $Rh(NO)_2$ in argon. The ratio of intensities calculated for the $^2B_1$ state using B3LYP is 1:10, in closer agreement with experiment than that for the nonplanar state, which is further evidence that the planar geometry is correct despite the negative frequency calculated using B3LYP.

IrNO. A sharp band at 1851.2 cm^{-1} in neon grows in on annealing but diminishes on photolysis (Figure 4). The $^{15}N^{16}O$ counterpart at 1810.7 cm^{-1} gives a ratio of 1.0224. This high ratio indicates a significant coupling between the Ir−N and N−O stretching modes that increases the amplitude of the nitrogen atom in the higher frequency vibration relative to that in isolated NO. The $^{15}N^{18}O$ counterpart to these bands was not observed owing to masking by $(^{15}N^{18}O)_2$.

The argon counterpart to this band is at 1838.7 cm^{-1} (Figure 5) is slightly lower than the neon value as is typically the case.[38] The $^{15}N^{16}O$ and $^{15}N^{18}O$ bands are observed at 1793.7 and 1759.3 cm^{-1}, respectively, giving $^{14}N^{16}O/^{15}N^{16}O$ and $^{15}N^{16}O/^{15}N^{18}O$ isotopic ratios of 1.0222 and 1.0197; the former is identical to that in neon within the accuracy of the measurement. Applying the latter ratio to the 1810.7 cm^{-1} band in neon indicates that the band due to $Ir^{15}N^{18}O$ should be at 1775.7 cm^{-1}, which is completely obscured by a band at 1775.5 cm^{-1} due to $^{15}N^{18}O$ and is therefore not observed. This region of the spectrum is clear enough to show that there are no intermediate components in the $^{14}N^{16}O + {}^{15}N^{16}O$/Ar experiment, indicating that only one

TABLE 8: Geometries, Energies, and Frequencies Calculated for Selected Neutral and Ionic Iridium Nitrosyls Using DFT (B3LYP/LanL2DZ/6-311+G(d))

molecule (ground state) [relative energy, kJ/mol]	$\langle S^2 \rangle$	geometry (Å deg)	frequencies (cm^{-1}) [intensities (km/mol)]	scale factors argon	scale factors neon
IrNO ($^1\Sigma^+$) [0]		IrN: 1.673; NO: 1.162 ∠IrNO: 180.0	1919.5 [663], 700.6 [5], 366.6 [14]	0.955	0.964
NIrO ($^1A'$) [+98]		IrN: 1.658; IrO: 1.747 ∠NIrO: 121.1	1119.5 [21], 875.3 [101], 293.2 [0]	0.873 0.972	0.888 0.993
NIrO ($^1A''$) [+99]	0.2096	IrN: 1.670; IrO: 1.766 ∠NIrO: 123.9	1070.8 [11], 785.1 [36], 274.1 [3]		
NIrO ($^3A'$) [+126]	2.0001	IrN: 1.671; IrO: 1.773 ∠NIrO: 140.2	1060.3 [30], 794.7 [66], 266.1 [4]		
NIrO ($^3A''$) [+263]	2.0098	IrN: 1.744; IrO: 1.812 ∠NIrO: 113.8	831.6 [13], 682.8 [2], 272.4 [8]		
$IrNO^+$ ($^2\Delta$) [0]	0.7504	IrN: 1.726; NO: 1.128 ∠NIrO: 180.0	2095.3 [612], 617.4 [12], 338.6 [8]		0.950
$IrNO^+$ ($^2\Sigma^+$) [+34]	0.7500	IrN: 1.739; NO: 1.123 ∠NIrO: 180.0	2061.0 [0], 630.2 [13], 369.3 [6]x2		
$Ir(NO)_2$ ($^2B_1$) [0]	0.7523	IrN: 1.789; NO: 1.163 ∠NIrN: 139.9 ∠IrNO: 167.6	1912.2 [151], 1834.1 [1934], 622.7 [3], 546.6 [3], 468.6 [0]...80.4 [1]	0.950	
$Ir(NO)_2$ ($^2A_1$) [+13]	0.7624	IrN: 1.798; NO: 1.164 ∠NIrN: 143.8 ∠IrNO: 161.3	1902.1 [143], 1824.7 [1792], 738.7 [40], 569.9 [1], 484.1 [5], 400.7 [1]...65.7 [1]		
$Ir(NO)_2$ $(\delta)^1(\pi)^2$ [+37]	3.7514	IrN: 1.826; NO: 1.168 ∠NIrN: 180.0 ∠IrNO: 180.0	1905.4 [0], 1828.1 [1903], 545.1 [0], 422.6 [35], 418.6 [2]...69.5 [0]		
$Ir(NO)_3$ $''^1A''$ [+21]		IrN: 1.820; NO: 1.160 ∠NIrN: 120.0 ∠IrNO: 180.0	1913.9 [0], 1838.3 [1840]x2, 605.5 [69]x2, 571.5 [48], 546.7 [0], 437.3 [53]x2...46.2 [0]		
$Ir(NO)_3$ $''^3A''$ [0]	2.0182	IrN: 1.834; NO: 1.166 ∠NIrN: 120.0 ∠IrNO: 180.0	1883.7 [0], 1822.3 [1542]x2, 534.0 [11]x2, 519.7 [0], 508.4 [8]...−17.4 [4]	0.958	0.962

TABLE 9: Reaction Energies Calculated Using DFT

reaction	ΔE(BPW91)/(kJ/mol)	ΔE(B3LYP)/(kJ/mol)	reaction no.
RhNO ($^2A'$) + NO ($^2\Pi$) → $Rh(NO)_2$ ($^2B_1$)	−197	−144	1
$Rh(NO)_2$ ($^2B_1$) + NO ($^2\Pi$) → $Rh(NO)_3$ ($''^1A''$)	−120	−44	2
IrNO ($^2\Sigma^+$) + NO ($^2\Pi$) → $Ir(NO)_2$ ($^2B_1$)	−271	−218	3
$Ir(NO)_2$ ($^2B_1$) + NO ($^2\Pi$) → $Ir(NO)_3$ ($''^1A''$)	−169	−101	4

TABLE 10: Force Constants (N m^{-1}) and Bond Angles (deg) Calculated for NIrO and NRhO Using Experimental Data

	f_{M-N}		f_{M-O}		$f_{M-N/M-O}$		bond angle	
metal	mean	std dev	mean	std dev	mean	std dev	mean	std dev
Ir	720	5	656	10				
Rh	675	1	541	1	5	11	90	12

TABLE 11: Comparison of Force Constants (N m^{-1}) Calculated for NMN, OMO, and NMO (M = Ir, Rh)

		iridium		rhodium	
molecule	bond	f_{M-X}	$f_{M-X/M-Y}$	f_{M-X}	$f_{M-X/M-Y}$
NMN	M−N	638[a]	89[a]	533[b]	69[b]
NMO	M−N	720		675	5
	M−O	656		541	
OMO	M−O	765[c]	66[c]	628[c]	45[c]

[a] NIrN in solid nitrogen, unpublished results. [b] From ref 36. [c] From ref 39.

NO subunit is involved and supporting the assignment of these bands to IrNO.

The DFT calculations for IrNO are in good agreement with experiment. The $^1\Sigma^+$ singlet ground state is found to be linear with both BPW91 and B3LYP density functionals; and the triplet and other singlet states are considerably higher in energy. The NO stretching frequency of 1878.9 cm^{-1} calculated with BPW91 is 43.1 cm^{-1} higher than observed in argon, and the B3LYP calculated frequency requires a scale factor of 0.955. These frequencies are consistent with the results for other metal nitrosyls studied in this laboratory.[24,25] More importantly, the calculated $^{14}N^{16}O/^{15}N^{16}O$ and $^{15}N^{16}O/^{15}N^{18}O$ ratios of 1.0230, 1.0195 (BPW91) and 1.0227, 1.0202 (B3LYP) are in good agreement with experiment (1.0222, 1.0197), showing that DFT has described the properties of IrNO correctly.

$Ir(NO)_3$. A sharp band at 1745.3 cm^{-1} in argon exhibits strong growth during annealing and moderate growth during photolysis (Figure 5). Weak bands at 3550.3 and 3479.9 cm^{-1} track with this band under all conditions. When the experiment is repeated with an equal mixture of $^{14}N^{16}O$ and $^{15}N^{16}O$, the 1745.3 cm^{-1} band is replaced by a quartet characteristic of the degenerate mode of a molecule[26] with a 3-fold symmetry axis (Figure 6). Accordingly, the 1745.3 cm^{-1} band is assigned to the degenerate nitrosyl stretching mode of $Ir(NO)_3$. The weaker band at 3479.9 cm^{-1} is slightly less than double the fundamental frequency and is therefore assigned to the first overtone of that mode, the 10.7 cm^{-1} difference arising from anharmonicity. The band at 3550.3 cm^{-1} is assigned to the combination of the symmetric and degenerate modes, and if the same anharmonicity is assumed then the symmetric nitrosyl stretching frequency is estimated to be 1815.5 cm^{-1}, assuming the same matrix shifts for the two modes. Two intermediate components were observed in the mixed isotopic experiment for the 3479.9 cm^{-1} band, resulting in a 13:5:10:5 intensity pattern, very different to the 5:3:3:5 intensity pattern observed for the fundamental of the degenerate mode. The 3550.3 cm^{-1} band is weaker, and no

intermediate components are discernible in the mixed isotopic experiment.

$Ir(NO)_3$ was observed at 1753.7 cm^{-1} in neon, but the quartet of peaks could not be resolved in the mixed isotopic experiment due to the intense triplet of bands arising from $(NO)_2$, and $Ir(NO)_2$ (see below).

The DFT calculations using the BPW91 functional for $Ir(NO)_3$ produce frequencies in good agreement with experiment, though the ground state is uncertain since the singlet and triplet states are within 11 kJ/mol and both give nitrosyl stretching frequencies that are compatible with experiment; the singlet state frequencies for the symmetric and degenerate stretching modes are 25.9 and 35.6 cm^{-1} higher than the argon values, and the triplet state frequencies are 4.0 and 22.1 cm^{-1} higher. When the calculations are repeated with the B3LYP functional, the triplet state is 21 kJ/mol *lower* in energy, and the frequencies for both states require scale factors in the range 0.94−0.96.[24,25] The singlet state frequencies are more in line with previous results for metal nitrosyls, but the triplet frequencies are also reasonable and cannot be ruled out. In all cases the molecule adopts a trigonal planar structure slightly distorted from D_{3h}. The $^{14}N^{16}O/^{15}N^{16}O$ and $^{15}N^{16}O/^{15}N^{18}O$ ratios are the same for each calculation, 1.0206 and 1.0240, respectively, in good agreement with the experimental values 1.0202 and 1.0235. This molecule and the rhodium analogue $Rh(NO)_3$ have formal electron counts of 18 and are therefore the most highly coordinated nitrosyl complexes that can be isolated for these metals. Higher coordination is possible if one or more nitrosyl ligands adopt a bent configuration, as was observed for the copper nitrosyls,[23] but there is no evidence for this in the rhodium or iridium nitrosyls.

$Ir(NO)_2$. Given the abundance of IrNO and $Ir(NO)_3$ in the argon and neon matrices, it is logical that $Ir(NO)_2$ should also be present. Close examination of the NO/Ar spectra reveals features close to the $Ir(NO)_3$ bands that are consistent with the expected behavior of $Ir(NO)_2$; three weak bands at 1743.2, 1741.4, and 1737.3 cm^{-1}, not present initially, grow in during low-temperature annealing and photolysis, and decrease on higher temperature annealing. These bands, and the $^{15}N^{16}O$/Ar and $^{15}N^{18}O$/Ar counterparts at 1708.4, 1707.0, 1702.6 cm^{-1}, and 1669.5, 1667.9, 1663.7 cm^{-1}, respectively, could simply be matrix sites for $Ir(NO)_3$. However, the $^{14}N^{16}O + {}^{15}N^{16}O$/Ar mixed isotope experiment suggests otherwise (Figure 6). If the above bands were simply different matrix sites for $Ir(NO)_3$, they must be present for each of the intermediate bands at 1729.6 and 1719.5 cm^{-1} due to $Ir(^{14}N^{16}O)(^{15}N^{16}O)_2$ and $Ir(^{14}N^{16}O)_2(^{15}N^{16}O)$ respectively, but this is not the case. Weak bands 1721.3 and 1715.8 cm^{-1} in this experiment track with the 1708.4 and 1702.6 cm^{-1} bands; the third band is obscured by the large 1719.5 cm^{-1} band. These are more intense than either of the pure isotope bands, and the approximate 1:2:1 intensity profile is appropriate for the out-of-phase nitrosyl stretching mode of $Ir(NO)_2$. The neon spectra are unclear since the $Ir(NO)_3$ band is broad and has at least two matrix sites. No reasonable candidates for the dinitrosyl are observed in neon, but it is likely that they are coincident with the absorptions due to $Ir(NO)_3$ and cannot be distinguished. As noted above, the mixed isotopic $^{14}N^{16}O + {}^{15}N^{18}O$/Ne spectra are complicated by the large site-split triplet of bands due to $(NO)_2$, and no definitive assignments for the $Ir(NO)_2$ and $Ir(NO)_3$ intermediates can be made.

The DFT calculations for this species add support to the assignment, although the correct ground state is again ambiguous. Both functionals find the planar $^2A_1$ and $^2B_1$ states to be of similar energy with the $^2B_1$ state slightly lower; the quartet states are much higher energy and may be ignored. The antisymmetric stretching modes calculated for these states with the BPW91 functional are 1779.0 and 1778.2 cm^{-1}, higher than the experimental value of 1736.5 cm^{-1} in argon. These are of the expected accuracy for this functional, and either could be the ground state. Similarly, the frequencies calculated with B3LYP are almost identical and no distinction can be made. The ground state for $Rh(NO)_2$ described above is determined to be $^2B_1$, though this need not be the case for $Ir(NO)_2$.

The $^{14}N^{16}O/^{15}N^{16}O$ and $^{15}N^{16}O/^{15}N^{18}O$ isotopic ratios are calculated to be 1.0205 ± 0.0001 and 1.0240 ± 0.0002 with either state, in good agreement with the experimental values of 1.0204 and 1.0233, and the antisymmetric stretching frequency of $Ir(^{14}N^{16}O)(^{15}N^{16}O)$ is calculated to be 4−5 cm^{-1} below the midpoint of the pure isotope bands for both states with the BPW91 functional, also in good agreement with the experimental value of 4.5 cm^{-1}. Unfortunately, the yield of $Ir(NO)_2$ is much less than that of $Rh(NO)_2$, and so bands due to the symmetric stretch, calculated to be much weaker, are not observed. Using the results for $Rh(NO)_2$ as a guide, the frequency expected for this mode is 1825 ± 10 cm^{-1} in argon.

Reaction Energies. The energies for the addition reactions that give the $M(NO)_2$ and $M(NO)_3$ complexes are listed in Table 9. All are exothermic, as expected from the growth of these species on annealing. This growth also shows that no appreciable activation energy is required for these reactions to occur. The reactions for the iridium species release more energy, in agreement with the stronger metal−ligand binding expected for the third row transition metal.

$RhNO^+$ and $IrNO^+$. A sharp, weak band at 1957.5 cm^{-1} in Rh/neon experiments grows in during annealing but diminishes on photolysis (Figure 1). The $^{15}N^{16}O$ and $^{15}N^{18}O$ counterparts at 1919.9 and 1873.9 cm^{-1} give ratios of 1.0196 and 1.0245, respectively. No intermediate band is observed in the $^{14}N^{16}O + {}^{15}N^{16}O$/Ne experiment, indicating that only one NO subunit is involved in the mode. These bands were not observed in argon. Based on the numerous studies of transition metals and nitric oxide in this laboratory, the straightforward assignment is to the molecular cation $RhNO^+$.[16−26] The intensity of the 1957.5 cm^{-1} band in neon is increased by a factor of 2 with respect to the RhNO band when the reagent gas is doped with CCl_4, which captures electrons, enhances the survival of Rh^+ cations and supports this assignment. A similar effect has been observed for other MNO^+ cations.[24,26]

Our DFT calculations for $RhNO^+$ strengthen this assignment: both BPW91 and B3LYP predict a $^2\Sigma^+$ ground state, with nitrosyl stretching frequencies of 1990.8 and 2087.4 cm^{-1}, respectively. The former is 33.3 cm^{-1} higher than the neon value, and the latter requires a scale factor of 0.938, typical values for metal nitrosyls.[24,25] Attempts to find other doublet states of comparable energy were unsuccessful with both functionals, and $^2\Sigma^+$ is identified as the ground state for $RhNO^+$.

$IrNO^+$ is observed in neon at 1990.0 cm^{-1}, with a $^{15}N^{16}O$ counterpart at 1949.5 cm^{-1} to give a ratio of 1.0208 (Figure 4). The yields of iridium nitrosyl products in the $^{15}N^{18}O$/Ne experiment were too low to observe the absorption due to $Ir^{15}N^{18}O^+$, but all three absorptions were observed in the argon experiments at 1980.1, 1939.7, and 1896.7 cm^{-1}, with isotopic ratios of 1.0208 and 1.0227. The DFT calculations for $IrNO^+$ completely support this assignment, although there is uncertainty as to which is the correct ground state. The lowest energy state calculated using the BPW91 functional is $^2\Delta$, with a nitrosyl stretching frequency of 2023.9 cm^{-1}. This is 43.8 cm^{-1} higher than the argon value, a typical result for this functional,[24,25] and

the calculated isotopic ratios of 1.0211 and 1.0230 are in agreement with experiment. The B3LYP functional also finds the $^2\Delta$ state to be lowest in energy, with a stretching frequency of 2095.3 cm^{-1}. This requires a scale factor of 0.945, also consistent with previous calculations of metal nitrosyls. However, a $^2\Sigma^+$ state is only 28 kJ/mol higher in energy using BPW91, and 34 kJ/mol higher with the B3LYP functional, and must also be considered for the ground state. The NO stretching frequency of 1993.1 cm^{-1} calculated for this state using the BPW91 functional is in very good agreement with experiment, but as noted above, this functional tends to give nitrosyl frequencies a few tens of wavenumbers too high and the apparent agreement actually disfavors the assignment. It is clear from these results that the calculations support assignment of the observed band to linear $IrNO^+$ in a $^2\Delta$ ground state, although the $^2\Sigma^+$ state cannot be ruled out. It is noteworthy that the isotopic ratios for both $RhNO^+$ and $IrNO^+$ are different from those in the neutral molecules, exhibiting less nitrogen and more oxygen participation in the nitrosyl stretching mode; clearly mode mixing is less in the cations than in the neutral molecules.

NRhO and NIrO. For Rh sharp, weak bands are observed at 964.2 and 813.7 cm^{-1} in argon (Figure 7), and only the upper band is observed at 965.4 cm^{-1} in neon. The $^{14}N^{16}O/^{15}N^{16}O$ ratio of 1.0305 for the upper band and the $^{15}N^{16}O/^{15}N^{18}O$ ratio of 1.0517 for the lower band are almost identical to the respective Rh−N and Rh−O harmonic diatomic values of 1.0306 and 1.0520 indicating that the observed bands are due to Rh−N and Rh−O stretching modes and the NRhO molecule must be considered. This class of molecule has been observed in most metal nitrosyl systems investigated in this laboratory, and the physical properties in this series were recently summarized.[25] NRhO is unusual in that the relative intensities of the observed bands are 1.5:1, with the higher frequency band being more intense. The lower frequency band due to the M−O stretching mode is more intense in most other NMO molecules.[16−22]

The DFT calculations for NRhO are less complicated than those described for NIrO below and are more effective in reproducing the experimental observations. The $^1A'$ state is substantially lower in energy than the $^1A''$, $^3A'$, and $^3A''$ states, and the stretching frequencies of 1017.2 and 826.1 cm^{-1} calculated for this state are 53.0 and 12.4 cm^{-1} higher than the observed bands. The B3LYP results are equally clear-cut: $^1A'$ is the lowest energy state and the calculated frequencies require scale factors of 0.909 and 0.940, again typical for this type of molecule. In addition, the calculated $^{14}N^{16}O/^{15}N^{16}O$ and $^{15}N^{16}O/^{15}N^{18}O$ ratios for the Rh−N and Rh−O stretching modes of 1.0305 and 1.0524 are in very good agreement with the experimental values of 1.0305 and 1.0517. Finally, the calculated intensities of 1.1:1 (BPW91) and 1:1 (B3LYP) are in good agreement with the experimental value of 1.4:1, reflecting the unusually large intensity observed for the Rh−N stretching mode.

The analogous NIrO bands are observed at 977.3 and 850.6 cm^{-1} in argon, and the latter band is 5.5 times more intense (Figure 8). Weaker matrix sites at 975.3 and 852.6 cm^{-1} disappear during annealing. The higher frequency band exhibits a large $^{14}N^{16}O/^{15}N^{16}O$ ratio of 1.0267, but a very small $^{15}N^{16}O/^{15}N^{18}O$ ratio of 1.0052. Conversely, the band at 850.6 cm^{-1} has ratios of 1.0031 and 1.0448. The 1.0267 and 1.0448 ratios are comparable to the harmonic ratios of 1.0325 and 1.0557 expected for Ir−N and Ir−O stretching modes, indicating that the observed modes are predominantly Ir−N and Ir−O stretching vibrations, but with significant coupling between the modes. As expected, the $^{14}N^{16}O + {}^{15}N^{16}O$/Ar mixed isotope experiment shows only doublets with no intermediate components (Figure 8). The neon counterparts to these bands are observed at 994.6 and 868.9 cm^{-1}, about 18 cm^{-1} higher than the argon values.

The DFT results for NIrO are complicated since three different states, $^1A'$, $^1A''$, and $^3A''$, are calculated to have energies within 22 kJ/mol of each other with the BPW91 functional: the $^3A''$ state is lowest by only 4 kJ/mol (Table 7). The $^3A'$ state is 56 kJ/mol higher in energy than the $^3A''$ state and can probably be ignored. Previous DFT calculations on this class of molecule are less accurate than those for the simpler nitrosyl complexes: the M−N stretching frequency is usually overestimated by several tens of wavenumbers, whereas the lower M−O stretching frequency is slightly higher than the observed value (in argon).[24,25] Using this as a guide to the expected accuracy of the NIrO calculations, the $^1A'$ state is the best candidate for the ground state since the predicted Ir−N and Ir−O stretching modes are 98.7 and 6.3 cm^{-1} higher than the argon values. The B3LYP calculations for NIrO support this conclusion (Table 8), as the $^1A'$ state has the lowest energy and the stretching frequencies require scale factors less than one. The Ir−O stretching frequency calculated for the $^1A''$ and $^3A'$ states, which are energetically competitive with the $^1A'$ state, is *lower* than the experimental value, which is not usually the case with the B3LYP functional. Finally, the $^3A''$ state may be disregarded since it is 165 kJ/mol higher in energy than the $^1A'$ state with this functional, and has frequencies that are much lower than the experimental values. The $^1A'$ state is therefore identified as the ground state for NIrO. However, the calculated $^{14}N^{16}O/^{15}N^{16}O$ ratio of 1.0316 for the higher frequency stretching mode and $^{15}N^{16}O/^{15}N^{18}O$ ratio of 1.0539 for the lower frequency stretching mode (all calculations) are in poor agreement with the observed values of 1.0267 and 1.0448. The DFT values approach the harmonic diatomic limits of 1.0325 and 1.0557 for isolated Ir−N and Ir−O, which shows that DFT has underestimated the degree of mode mixing in NIrO. Despite this deficiency, the relative intensities of the stretching modes, calculated to be 1:4.5 (BPW91) and 1:4.8 (B3LYP), are in good agreement with the observed intensity ratio of 1:5.5.

Both NIrO and NRhO are less stable than the IrNO and RhNO isomers, which is usually the case for NMO molecules.[16−22] An important exception is NOsO, which was calculated to be more stable than OsNO. This was attributed to the exceptionally strong Os−N and Os−O bonds in NOsO, as reflected in the experimentally derived force constants of 849 and 710 Nm^{-1}, the largest values for any NMO molecule.[25] The force constants for NRhO and NIrO are calculated in the same way and the results are summarized in Table 10. These were calculated by neglecting the bending mode and solving for the M−N and M−O force constants, the stretch−stretch interaction constant, and the bond angle in 12 sets of equations. There is little uncertainty in the Rh−N and Rh−O force constants, and these may be considered reliable within the model used. The interaction force constant is close to zero, and the bond angle is near 90°, but the uncertainties in these quantities are large. It proved more difficult to determine best fit values for NIrO, as reflected in the greater uncertainty in the force constants. The two remaining parameters were so variable that no meaningful best fit values could be found.

The force constants and presumably the bonds are clearly stronger in NIrO than in NRhO, which is the usual trend for metal−ligand bonds down a transition metal group. This is also reflected in the smaller energy separation between IrNO and NIrO (69 kJ/mol, BPW91) than between RhNO and NRhO (203

kJ/mol, BPW91). The NCoO molecule was not observed in recent matrix isolation studies in this laboratory,[26] and this is probably because the Co−N and Co−O bonds are not strong enough to prevent dissociation. Group 9 is the latest transition metal group for which NMO molecules are observed owing to a decrease in M−N and M−O bond strengths along the row after the iron group metals caused by the increasing population of antibonding orbitals. Both NIrO and NRhO show growth on early annealing in argon, but bands at 929.1 and 900.0 cm^{-1} due to OIrO and ORhO, respectively,[39,40] also appear, so the increase is probably due to atom addition reactions rather than insertion by the metal into the N−O bond. Finally, the yield of NRhO is unaffected by photolysis; this is in contrast to NOsO, which was enhanced by irradiation via isomerization of OsNO.

It is also useful to compare the force constants in the insertion products with the corresponding dinitride and dioxide molecules, as shown in Table 11. In both cases, the M−N force constant and presumably the bond in NMO is stronger than that in NMN, and the M−O bond is weaker than that in OMO. The same relationship was observed for the osmium and ruthenium analogues,[25] which was explained by the smaller energy difference between the metal and nitrogen orbitals in the NMO molecule, strengthening the M−N interaction at the expense of the M−O bond.

$Rh_x(NO)_y$ and $Ir_x(NO)_y$. Weaker bands that grow on annealing are observed below those due to the metal nitrosyls that are probably due to metal cluster species that involve two or more metal atoms. These are marked in the data tables as $Rh_x(NO)_y$ and $Ir_x(NO)_y$, and no specific assignments are proposed.

Surface Chemistry. When NO is adsorbed on Ir(111) at sufficiently high coverage, a loss feature is observed at 1860 cm^{-1} in EEL spectra that is most likely due to NO in a top site,[11] with an analogous band observed near 1840 cm^{-1} on Ir(100).[12] These are very close to the values of 1851.1 and 1835.8 cm^{-1} observed for isolated IrNO in neon and argon. In addition, a 1958 cm^{-1} feature on Ir(100) assigned to a species with substantial positive character is intermediate between the 1851.1 and 1993.3 cm^{-1} bands assigned to IrNO and $IrNO^+$ in neon.[12] If a linear scale is assumed, the effective positive charge on the surface species is estimated to be 0.7−0.8.

Good agreement is also found between the vibrational data for isolated and surface rhodium nitrosyls. Nitric oxide absorbs at 1830 cm^{-1} on top sites of Rh(111) at sufficiently high coverages.[2,3] This is quite close to the 1806.4 cm^{-1} band due to RhNO in neon, though the argon value of 1775.1 cm^{-1} is considerably lower. Bands at 1920 and 1900 cm^{-1} on Ce−Rh/SiO_2 and Rh/Al_2O_3 assigned to NO^+ surface species are intermediate between the 1957.5 and 1806.4 cm^{-1} bands assigned to $RhNO^+$ and RhNO in neon,[4,5] which implies effective positive charges in the range 0.6−0.8. In addition, bands were observed at 1825 and 1743 cm^{-1} on Rh/Al_2O_3 and were assigned to the symmetric and asymmetric stretching modes of Rh$(NO)_2$/Al_2O_3 on the basis of mixed isotopic data. The latter band is very close to the bands in neon and argon at 1746.9 and 1736.5 cm^{-1} assigned to isolated Rh$(NO)_2$.[6] These bands have a constant relative ratio of approximately 1:3 which indicates that the angle between the NO groups is close to 120°, within the bond dipole approximation.[41] This is in qualitative agreement with the values of 128.0° (BPW91) and 132.7° (B3LYP) calculated for ∠NRhN in Rh$(NO)_2$ using DFT, though the angle between the NO bonds is much less since the RhNO subunits are bent toward each other. Finally, bands in the 1600−1500 cm^{-1} region on Rh(111) have been assigned to NO in two- or three-fold bridge sites, which correspond to the weak bands in the present work assigned to $Rh_x(NO)_y$ cluster species.

Conclusions

Laser-ablated rhodium and iridium atoms were reacted with nitric oxide and the products were isolated in solid argon and neon. The nitrosyl complexes Rh$(NO)_{1-3}$ and Ir$(NO)_{1-3}$ were the major products with the trinitrosyls Rh$(NO)_3$ and Ir$(NO)_3$ the most abundant. The mononitrosyl cations $RhNO^+$ and $IrNO^+$ were also observed. Our DFT calculations for these species effectively reproduced the experimental observations and demonstrated the same level of accuracy found for previous transition metal nitrosyl complexes.[24,25] However, RhNO is calculated to be nonlinear with both BPW91 and B3LYP functionals when the linear geometry is more likely to be correct. Similarly, Rh$(NO)_2$ is predicted to adopt a nonplanar geometry using the B3LYP functional, but a planar geometry with the BPW91 functional. The latter is found to be a better fit to the experimental data, and the B3LYP calculation is qualitatively incorrect. Similar problems were encountered in DFT calculations for ORhO, which incorrectly predict a bent geometry.[39] These results should be considered in future DFT calculations for rhodium. No such problems were encountered in the iridium nitrosyl calculations.

The stretching frequencies for the isolated metal nitrosyls reported here are found to correlate well with those due to nitrosyl products observed on rhodium and iridium surfaces, typically agreeing to within a few tens of wavenumbers. This may prove useful in identifying dinitrosyl and trinitrosyl surface species.

Finally, the insertion products NRhO and NIrO are also observed and effectively modeled by DFT. Force constant calculations suggest that the M−N and M−O bonds are stronger in NIrO than in NRhO, which is expected from similar calculations for other NMO molecules.[25]

Acknowledgment. We gratefully acknowledge research support from the Petroleum Research Fund.

References and Notes

(1) Brown, W. A.; King, D. A. *J. Phys. Chem. B* **2000**, *104*, 2578.
(2) Kim, Y. J.; Thevuthasan, S.; Herman, G. S.; Peden, C. H. F.; Chambers, S. A.; Belton, D. N.; Permana, H. *Surf. Sci.* **1996**, *359*, 269.
(3) Kao, C. T.; Blackman, G. S.; Van Hove, M. A.; Somorjai, G. A. *Surf. Sci.* **1989**, *224*, 77.
(4) Srinivas, G.; Chuang, S. S. C.; Debnath, S. *J. Catal.* **1994**, *148*, 748.
(5) Almusaiteer, K. A.; Chuang, S. C. *J. Phys. Chem. B* **2000**, *104*, 2265.
(6) Liang, J.; Wang, H. P.; Spicer, L. D. *J. Phys. Chem.* **1985**, *89*, 5840.
(7) Loffreda, D.; Simon, D.; Sautet, P. *Chem. Phys. Lett.* **1998**, *291*, 15.
(8) Liao, D.; Glassford, K. M.; Ramprasad, R.; Adams, J. B. *Surf. Sci.* **1998**, *415*, 11.
(9) Chafik, T.; Kondarides, D. I.; Verykios, X. E. *J. Catal.* **2000**, *190*, 446.
(10) Gomez, R.; Weaver, M. J. *J. Phys. Chem. B* **1998**, *102*, 3754.
(11) Davis, J. E.; Karseboom, S. G.; Nolan, P. D.; Mullins, C. B. *J. Chem. Phys.* **1996**, *105*, 8362.
(12) Gardner, P.; Martin, R.; Nalezinski, R.; Lamont, C. L. A.; Weaver, M. J.; Bradshaw, A. M. *J. Chem. Soc., Faraday Trans.* **1995**, *91*, 3575.
(13) Zhou, M. F.; Andrews, L. *J. Am. Chem. Soc.* **1999**, *121*, 9171.
(14) Zhou, M. F.; Andrews, L. *J. Phys. Chem. A* **1999**, *103*, 7773.
(15) Morrow, B. A.; Baraton, M. I.; Roustan, J. L. *J. Am. Chem. Soc.* **1987**, *109*, 7541.
(16) Andrews, L.; Zhou, M. F.; Ball, D. W. *J. Phys. Chem. A* **1998**, *102*, 10041 (Mn, Re + NO).
(17) Zhou, M. F.; Andrews, L. *J. Phys. Chem. A* **1998**, *102*, 10025 (Nb, Ta + NO).

(18) Kushto, G.; Zhou, M. F.; Andrews, L. *J. Phys. Chem. A* **1999**, *103*, 1115 (Ti, Sc + NO).
(19) Kushto, G.; Andrews, L. *J. Phys. Chem. A* **1999**, *103*, 4836 (Ti, Zr, Hf + NO).
(20) Zhou, M. F.; Andrews, L. *J. Phys. Chem. A* **1998**, *103*, 478 (V + NO).
(21) Zhou, M. F.; Andrews, L. *J. Phys. Chem. A* **1998**, *102*, 7452 (Cr + NO).
(22) Andrews, L.; Zhou, M. F. *J. Phys. Chem. A* **1998**, *103*, 4167 (Mo, W + NO).
(23) Zhou, M. F.; Andrews, L. *J. Phys. Chem. A* **2000**, *104*, 2618 (Cu + NO).
(24) Citra, A.; Andrews, L. *J. Phys. Chem. A* **2000**, *104*, 8160 (Pt, Pd + NO).
(25) Citra, A.; Andrews, L. *J. Phys. Chem. A* **2000**, *104*, 8689 (Os, Ru + NO).
(26) Zhou, M. F.; Andrews, L. *J. Phys. Chem. A* **2000**, *104*, 3915 (Fe, Co, Ni + NO) and references therein.
(27) Burkholder, T. R.; Andrews, L. *J. Chem. Phys.* **1991**, *95*, 8697.
(28) Hassanzadeh, P.; Andrews, L. *J. Phys. Chem. A* **1992**, *96*, 9177.
(29) Frisch, M. J.; Trucks, G. W.; Schlegel, H. B.; Gill, P. M. W.; Johnson, B. G.; Robb, M. A.; Cheeseman, J. R.; Keith, T.; Petersson, G. A.; Montgomery, J. A.; Raghavachari, K.; Al-Laham, M. A.; Zakrzewski, V. G.; Ortiz, J. V.; Foresman, J. B.; Cioslowski, J.; Stefanov, B. B.; Nanayakkara, A.; Challacombe, M.; Peng, C. Y.; Ayala, P. Y.; Chen, W.; Wong, M. W.; Andres, J. L.; Replogle, E. S.; Gomperts, R.; Martin, R. L.; Fox, D. J.; Binkley, J. S.; Defrees, D. J.; Baker, J.; Stewart, J. P.; Head-Gordon, M.; Gonzalez, C.; Pople, J. A. *Gaussian 94*, Revision B.1; Gaussian, Inc.: Pittsburgh, PA, 1995.
(30) Becke, A. D. *Phys. Rev. A* **1988**, *38*, 3098.
(31) Perdew, J. P.; Wang, Y. *Phys. Rev. B* **1992**, *45*, 13244.
(32) Becke, A. D. *J. Chem. Phys.* **1993**, *98*, 5648.
(33) Krishnan, R.; Binkley, J. S.; Seeger, R.; Pople, J. A. *J. Chem. Phys.* **1980**, *72*, 650.
(34) Wadt, W. R.; Hay, P. J. *J. Chem. Phys.* **1985**, *82*, 284.
(35) Hay, P. J.; Wadt, W. R. *J. Chem. Phys.* **1985**, *82*, 299.
(36) Citra, A.; Andrews, L. *J. Phys. Chem. A* **1999**, *103*, 3410 (Rh + N_2).
(37) Sherrill, C. D.; Lee, M. S.; Gordon, M. H. *Chem. Phys. Lett.* **1999**, *302*, 425.
(38) Jacox, M. E. *Chem. Phys.* **1994**, *189*, 149.
(39) Citra, A.; Andrews, L. *J. Phys. Chem. A* **1999**, *103*, 4845.
(40) Citra, A.; Andrews, L. *J. Phys. Chem. A* **1999**, *103*, 4182.
(41) Wilson, E. B. Jr.; Decius, J. C.; Cross, P. C. *Molecular Vibrations: The Theory of Infrared and Raman Vibrational Spectra*; McGraw-Hill: New York, 1955.